Non-monotonic friction due to water capillary adhesion and hydrogen bonding at multi-asperity interfaces

Liang Peng[1], Feng-Chun Hsia[1,2], Sander Woutersen[1], Mischa Bonn[1,3], Bart Weber[1,2] and Daniel Bonn[1]

[1] Van der Waals-Zeeman Institute, Institute of Physics, University of Amsterdam, Science Park 904, 1098 XH Amsterdam, The Netherlands

[2] Advanced Research Center for Nanolithography (ARCNL), Science Park 106, 1098 XG Amsterdam, The Netherlands

[3] Molecular Spectroscopy Department, Max Planck Institute for Polymer Research, Ackermannweg 10, Mainz 55128, Germany

Abstract: Capillary adhesion due to water adsorption from the air can contribute to friction, especially for smooth interfaces in humid environments. We show that for multi-asperity (naturally oxidized) Si-on-Si interfaces, the friction coefficient goes through a maximum as a function of relative humidity. An adhesion model based on the boundary element method (BEM) that takes the roughness of the interfaces into account reproduces this non-monotonic behavior very well. Remarkably, we find the dry friction to be significantly lower than the 'lubricated friction' with macroscopic amounts of water present. The difference is attributed to the hydrogen-bonding network across the interface. Accordingly, the lubricated friction increases significantly if the water is replaced by heavy water (D_2O) with stronger hydrogen bonding.

Key words: Capillary adhesion, water, friction, multi-asperity, bonding, relative humidity

The frictional properties of silicon-based materials have been of interest to researchers for several decades, given the importance of friction for technology development in the semiconductor industry, including, for instance, improving the efficiency and extending the lifetime of micro-electromechanical systems (MEMS)[1–3]. Silicon components are often exposed to humid environments where capillary adhesion can occur across interfaces. This capillary adhesion is a key factor in increasing friction, especially for interfaces that are smooth compared to the range of the adhesive interaction[4,5]. Therefore, a fundamental understanding of how capillary adhesion and friction evolve with relative humidity, particularly in multi-asperity systems, is essential to control friction and reduce wear from a technological perspective. Moreover, understanding how nanoscale adhesion and friction mechanisms manifest themselves at larger length scales remains a major scientific challenge.

Numerous experiments have been conducted to tackle challenges related to the increasing importance of capillary adhesion and friction in silicon systems. For hydrophilic (naturally oxidized) silicon, the humidity dependence of capillary adhesion and friction has been studied by atomic force microscopy (AFM) experiments: friction and adhesion first increase with increasing humidity and then decrease[6–8]. This non-monotonic humidity dependence has been attributed to the competing roles of the Laplace pressure and the meniscus size at the interface; the former decreases with increasing relative humidity while the latter increases with increasing relative humidity[9–11]. Furthermore, the ice-like structure of adsorbed water in humid conditions can strongly enhance nanoscale adhesion and friction at low humidities (below 40%-80%)[3,12,13]. At a larger scale, non-monotonic adhesion behavior as a function of water content has been observed for assemblies of sand grains (with SiO_2 surfaces similar to the silicon surfaces studied here)[14,15]. Here the non-monotonic behavior was attributed to the roughness of the surfaces: before adhesive water bridges can form, the water first fills the small pores between the asperities of the surface[16].

Despite substantial theoretical efforts[11,17–19], few experiments[20,21] have addressed the mechanisms underlying the humidity dependence of capillary adhesion and its relation with friction at multi-asperity interfaces. Two main complications exist. First, the direct measurement of the adhesive force is prohibited by the so-called adhesion paradox[22–24]: the elastic energy stored in asperities provides a repulsive force between the two surfaces that masks the adhesive force. Second, the friction experiments may induce wear, which, in turn, influences adhesion[4,5,25,26].

In this paper, we experimentally show that multi-asperity Si-on-Si friction increases with relative humidity in the range from 0% to 20% and decreases again when the relative humidity increases beyond 20%. The dependence of the friction at higher levels of relative humidity can be captured by a simple capillary adhesion model based on the boundary element method without adjustable parameters. With increasing relative humidity, the reduction in Laplace pressure, which controls the capillary adhesive force, drives the decrease of the friction coefficient. In addition, we find that the value of the friction coefficient for the completely dry case (no capillary bridges) is much lower than the completely immersed case, which also has no capillary bridges.

We interpret the strong dependence of the friction on the relative humidity below 20% in terms of the hydrogen bonding across the interface, which is strongly reduced at humidities below 20%, but of course remains present for the completely immersed case.

Silicon-on-silicon friction experiments were performed with a rheometer (DSR 502, Anton Paar) inside a customized humidity-controlled chamber, as shown in Fig.1. The partial pressure of water vapor or the relative humidity inside the chamber is controlled by a humidifier (MHG100, proUmid). Before the experiments, the silicon spheres were rinsed with ethanol and sonicated in Milli-Q water, followed by nitrogen flow drying. In the friction experiments, a clean, 3 mm-diameter rough silicon sphere was brought into contact with an as-received smooth p-doped silicon (100) wafer (University Wafer) with a native oxide layer. The surface chemistry during sliding may therefore be a complex mix of Si-Si, Si-SiO_2, and SiO_2-SiO_2, due to the wear and reformation of the thin oxide layers on the silicon. The contact was formed under a normal load of 50 mN after the relative humidity inside the chamber was dried to 0.6%. The approximate contact diameter at 50 mN normal force was calculated to be 20 μm based on the classical Hertzian contact theory. The sliding speed imposed by the rheometer was 100 nm/s in humidity-dependent experiments and varied from 0.1 μm/s to 100 μm/s in the velocity-dependent experiments. During the sliding experiments, the rheometer moves the sphere tangentially on the wafer while measuring both externally applied load ($F_{external}$) and friction force (F_f). The ratio of these two forces gives the friction coefficient (CoF), $\mu = {F_f}/{F_{external}}$. It is important to note that any adhesion exerted at the interface is 'hidden' in the sense that it may influence the measured friction force, but it does not contribute to the externally applied load. To minimize the influence of wear, sliding strokes were kept short at 3 μm (as shown in Fig.S1), and each stroke was measured at a previously untouched section on the substrate. After a few strokes, the CoF reached a steady state; we report the steady-state values of the CoF. The surface topography of the spheres was measured before and after friction experiments by laser-scanning confocal microscopy (Keyence VK-X1000) over an area of 212×283 μm^2 (XYZ resolution of 400 nm × 400 nm × 12 nm, respectively) to verify that only minimal wear occurred[4].

In the humidity-dependent friction experiments, we vary the relative humidity inside the chamber between 0.6% and 80%. The humidity is first increased and subsequently decreased again, in intervals of 20%. The CoF is measured at each relative humidity. Before each change in the humidity, the chamber was first dried for one hour, by lowering the relative humidity to 0.6%, to remove any residual water. After drying, the system was equilibrated at the target humidity level for one hour before starting the friction measurement. During drying and equilibration, the sphere was kept in contact with the substrate. At the end of the humidity-dependent friction experiments, the contact was immersed in deionized water and friction was measured. After all friction experiments were completed, the topography of the sphere apex within an area of 31.13×31.13 μm^2 was captured by tapping mode AFM (Dimension Icon, Bruker) with Si tips (RTESPA-300, Bruker). Contact calculations using the AFM topography as input were carried out using the Tribology Simulator (available at

https://www.tribonet.org/cmdownloads/tribosolver-2/)

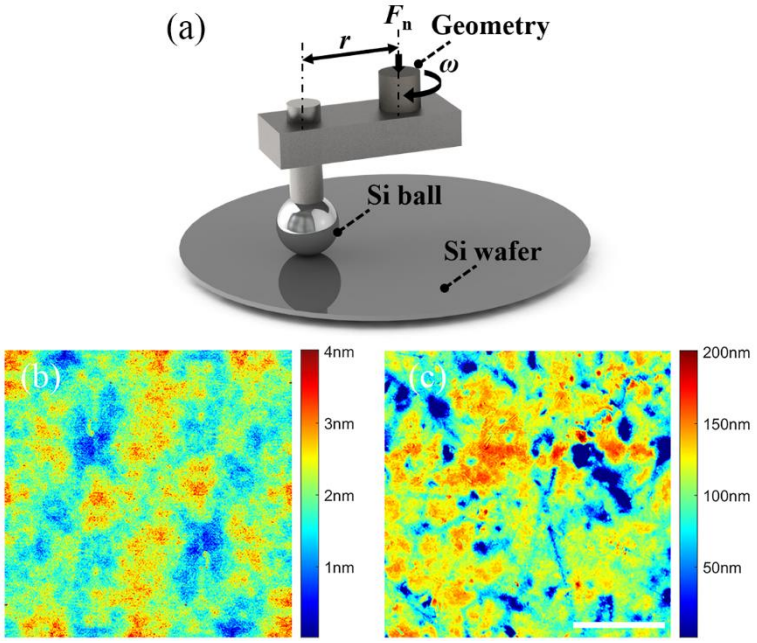

Fig.1 Experimental setup (a). A silicon ball inside a humidity-controlled chamber is clamped to the geometry of a rheometer which is used to measure normal and frictional forces between the silicon ball and the silicon wafer. The known distance between the rotation axis and the sphere, r = 12 mm, is used to translate the imposed rotation speed, ω, into a sliding speed and to translate the imposed torque into a friction force. AFM images of the wafer (b) and silicon ball (c) are shown. The root-mean-squared roughness of the surfaces was 0.5 nm (wafer) and 40.5 nm (sphere), measured over an area of 31.13×31.13 μm^2. Scale bar, 10 μm.

To investigate the effect of interfacial bonding on friction, velocity-dependent experiments (0.1 μm/s-100 μm/s) were conducted under dry and water-immersed conditions. Furthermore, the evolution of the CoF in time was also measured while the contact was immersed in heavy water (D_2O) instead of H_2O. The heavy water was free to exchange with water in the surrounding 60% relative humidity environment.

As shown in Fig. 2, the friction coefficient evolves with relative humidity without any hysteresis, and can be divided into two regimes. In the first regime, the CoF sharply increases when the relative humidity is increased from 0.6% to 20%. In the second regime, in which the relative humidity is between 20% and 80%, the friction decreases slightly with increasing relative humidity.

The observed non-monotonic behavior is well captured by a simple adhesion model (solid green line in Fig.2) which is detailed below. The adhesion model neglects the contribution of van der Waals forces to the adhesion, and only considers capillary adhesion[4,5]. As a result, the equilibrium of forces at the interface is given by Eq. (1).

$$\vec{F}_{adhesion} + \vec{F}_{external} + \vec{F}_{elastic} = 0 \quad (1)$$

where $\vec{F}_{adhesion}$, $\vec{F}_{external}$ and $\vec{F}_{elastic}$ are capillary adhesion, externally applied load, and elastic repulsive force, respectively. Multi-asperity adhesion is hard to detect, as

discussed above and shown in Fig. S3. To obtain a quantitative description, we employ boundary element method (BEM) contact calculations, in which the elasto-plastic equations are discretized and solved numerically to solve the contact problem and estimate the capillary adhesion. Both the capillary adhesion and the elastic force are calculated as a function of the average interfacial gap. We assume that the locally experienced adhesion forces influence the average interfacial gap in the same way as an externally applied force does. The Tribology Simulator can calculate the interface deformation associated with a given elastic repulsive force, $F_{elastic}$, using the measured surface topography and the mechanical properties of silicon (listed in Table S1). Subsequently, the adhesion force can be estimated based on the resulting interface geometry, which is described by the interfacial gap value as a function of the in-plane position.

To estimate the capillary adhesion force in the calculations, it is assumed that water bridges form within regions called capillary areas, where the local interfacial gap is below a threshold value, D. Within the capillary areas, there is capillary attraction due to the Laplace pressure difference between the inside and outside of the water bridges. The threshold value, D, is defined here as $D = 2 \times H + D_c$, in which H and D_c represent the absorbed water film thickness and the critical nucleation distance obtained from previous studies, as shown in Table S2[6,27,28]. The capillary adhesive force, $F_{simulated}^{adhesion}$, is calculated by multiplying the Laplace pressure with the capillary area. The external load can then be obtained from Eq. (1).

To describe the influence of the capillary adhesion, $\vec{F}_{adhesion}$ on friction, we assume that the measured friction force, $\vec{F}_f$, is proportional to the sum of the adhesion force, $\vec{F}_{adhesion}$, and the externally applied normal force, $\vec{F}_{external}$. This assumption is motivated by the observation of such 'load-controlled friction'[29,30] in similar systems[5,31]. The proportionality constant that links the friction force to the combined normal force, $|\vec{F}_{adhesion}| + |\vec{F}_{external}|$, can be obtained by performing a water immersed friction experiment in which there is no capillary adhesion, while the externally applied force and friction force can be measured. We thus obtain:

$$CoF_{simulated} = \frac{CoF_{immersed} \times |F_{external}| + CoF_{immersed} \times |F_{simulated}^{adhesion}|}{|F_{external}|}$$

$$= CoF_{immersed} + {|F_{simulated}^{adhesion}|}/{|F_{external}|} \times CoF_{immersed} \quad (2)$$

in which the $CoF_{simulated}$ is the estimated friction coefficient in the adhesion model and $CoF_{immersed}$ is the friction coefficient measured when the system is immersed in water such that there is no capillary adhesion.

The match between the simulation result and the experimental result obtained in the 20%-80% relative humidity regime shows that our proposed adhesion model,

without adjustable parameters, captures the non-monotonic change in friction with relative humidity. Capillary adhesion influences friction, and its impact depends on the superposition of two competing effects: growth of the capillary area and reduction of the Laplace pressure with increasing relative humidity. As the relative humidity increases, the range of the capillary adhesion, and thus the capillary area, increases due to the formation of thicker water layers[6] on the solid surfaces and due to the increased critical distance for capillary condensation, which scales with the (increasing) Kelvin radius[27]. The growing Kelvin radius, in turn, reduces the curvature of the liquid-gas interface, thereby reducing the Laplace pressure[6]. The non-monotonic change in friction as a function of relative humidity is analogous to the change in shear modulus of sand with water content[14,15]: a small amount of water enhances the attraction between sand grains by increasing capillary pressure; while too much water causes the merging of water bridges, destabilizing the sand finally. Similar non-monotonic friction trends, but with different mechanisms, have been explored at the carbon and graphite contact interface, where the non-monotonic change is dominated by contact quality or the number of pinning sites of intercalated water molecules[32]. For Si-on-Si multi-asperity friction at high relative humidities here, the reduction in Laplace pressure leads to the decrease in capillary adhesion and, thus, in friction coefficient. It should be noted that the precise dependence of the friction coefficient on relative humidity depends on the interface topography. The detailed estimates of capillary adhesive forces in various relative humidities are listed in Table S2.

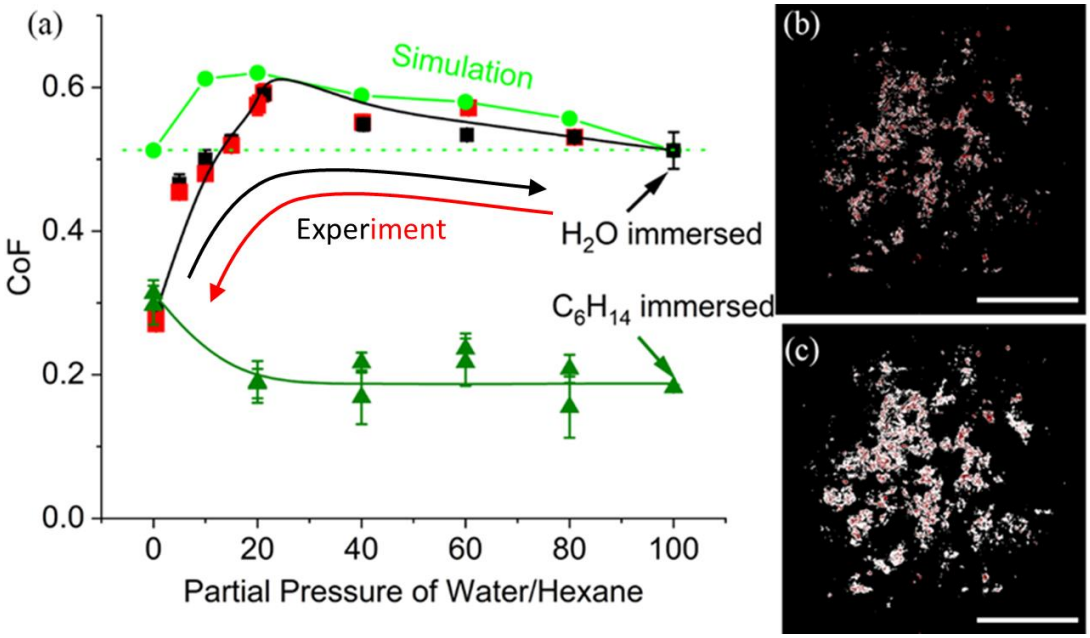

Fig.2 Friction as a function of relative humidity (RH) and partial pressure of hexane (a). Measurements were performed with increasing (black squares) and decreasing (red squares) relative humidity to rule out significant hysteresis. Furthermore, the data was collected in two separate experiments with different spheres (more experiments are reported in Fig. S4). The corresponding simulation result is represented by the solid green circles. The olive triangles in (a) display the evolution of the friction coefficient with the partial pressure of hexane at a sliding velocity of 1 μm/s . The hexane gas was introduced into the system after several sliding

strokes were performed in the dry environment (left-most data point). The relative humidity level for all hexane measurements was around 1%. Lines through the data points are drawn to guide the eye. (b) and (c) are two simulated contact maps under 20% RH (b) and 80% RH (c). The red, white, and black regions in the contact map correspond to the contact area, capillary area, and non-contact area without water bridges, respectively. Scale bar: 10 μm.

Despite the good agreement between measured and predicted CoF at high relative humidities (>20%), our adhesion model fails to predict the dramatic drop in friction coefficient observed at low (<20%) relative humidities. Also, the substantial difference in friction between the dry measurement and the water immersed measurement has not been observed previously in single asperity experiments[33,34]. Capillary adhesion cannot explain this difference in friction since there is no capillary adhesion in either the dry or water-immersed environments. Furthermore, hydrodynamic lubrication can be excluded since the sliding system runs in the boundary lubrication regime considering the low sliding speed (0.1 μm/s) and high contact pressure (3 GPa) in combination with the low viscosity of water (1.0×10^{-3} Pa s at 20°C).

We propose that the difference in friction measured at 0.6% RH and in the water-immersed condition originates from physical or covalent interfacial bonding associated with the presence of water[35–37]. That this is specific to water follows from a reference experiment performed in hexane vapor, where, in fact, the 1 % RH friction is lowered by the addition of hexane vapor, and the strong asymmetry between the friction measured in hexane vapor and hexane immersion is absent (Fig. 2). This suggests that hydrogen bonding may play an important role whenever water is present. To test this hypothesis further, we repeat the experiments using heavy water (D_2O) instead of water, the former having significantly stronger hydrogen bonds[38,39]. We therefore carry out an immersed friction experiment using heavy water, and indeed find that the friction is 14% ± 5% higher. This increase cannot be due to the higher viscosity of D_2O, since the viscous contribution to the friction is negligible at the velocities used in our experiments (see previous paragraph). To demonstrate that the higher friction of the heavy-water immersed contact is not due to experimental variability, we use the fact that D_2O exchanges easily with H_2O from humid air. We therefore repeat the experiment starting with a D_2O lubricated contact and introducing H_2O-humid air into the experimental chamber. As shown in the inset of Fig.3, the friction coefficient gradually decreases from $\mu = 0.58$ to $\mu = 0.51$ as heavy water exchanges with normal water from the surrounding air in two subsequent experiments. Similar rapid H/D exchange has been described in hydroxyl accessibility studies of deuterated wood[40]. The higher friction at the heavy water immersed interface can be attributed to the stronger hydrogen bonding compared to H_2O[38,39,41] . As heavy water at the interface is gradually replaced by normal water from the humid environment, the friction decreases due to the weaker interfacial hydrogen bond network. The interplay between the hydrogen bond network and adhesion has previously been demonstrated in AFM studies on silica through manipulating the solvent pH[42,43].

The assumption that the hydrogen bonding contributes to the friction is also supported by our velocity-dependent experiments, as shown in Fig.3. An approximately linear increase in friction with the logarithm of the sliding velocity is observed in the

velocity range from 0.1 μm/s to 100 μm/s in the dry environment (0.6% RH). The velocity strengthening of the dry friction is commonly attributed to thermally activated slip in which the shear stress lowers the activation barrier[44]. A spectacular observation is that the friction of the fully immersed contact shows a *decreasing* CoF with increasing velocity, exactly the opposite of the dry friction. As explained before, viscous effects such as hydrodynamic lubrication cannot take place at such low sliding velocities and high contact pressures. It is tempting to attribute the velocity-weakening friction to the dynamic equilibrium between the rupture and formation of the hydrogen-bonding network at the interface[45]. As the velocity increases, the rate at which interfacial hydrogen bonds are broken outpaces the rate at which interfacial hydrogen bonds are formed, thus leading to a smaller friction force. We can, very roughly, quantify this idea as follows. Given the typical length and formation time of a hydrogen bond in water (order of magnitude 1 nm and 1 ps, respectively)[46], we expect that at velocities above order 10^3 m/s, H-bond formation should no longer contribute significantly to the friction. This expectation is indeed supported by the extrapolated velocity dependence in water immersed friction measurements, in which the friction is predicted to be as low as 0.11±0.05 at a velocity of 10^3 m/s. Indeed this is comparable to the velocity-independent friction measured under hexane-immersed conditions, further corroborating our interpretation, as there would be no interfacial hydrogen bonding facilitated by the alkane.

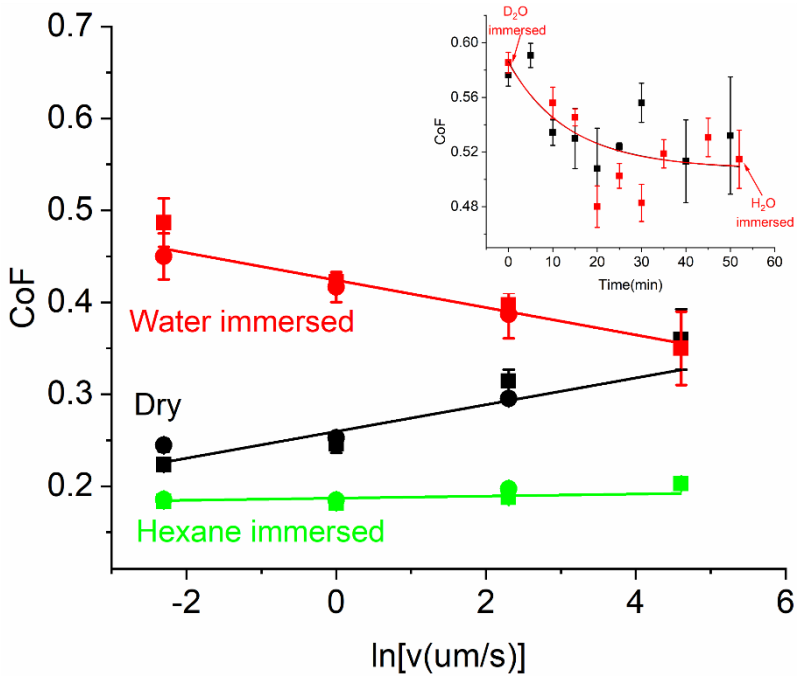

Fig.3 Dependence of the friction coefficient on sliding velocity. The red, black, and green data correspond to the friction coefficient measured at increasing (squares) and decreasing (solid circles) velocities ranging from 0.1 μm/s-100 μm/s in the dry case (relative humidity=0.6%), the water immersed case, and hexane-immersed case, respectively. The inset displays the change in friction coefficient as a function of time, measured as the D_2O immersed contact evolves into an H_2O immersed contact. In the inset, the red and black colored data points (squares) correspond to two independent experiments.

In conclusion, we have investigated the evolution of capillary adhesion and friction with relative humidity in a multi-asperity Si-on-Si system: the coefficient of friction first increases sharply in the relative humidity range from 0% to 20%, and then decreases slightly with increasing relative humidity at humidities above 20%. This evolution of the coefficient of friction with relative humidity can be influenced by drying hysteresis. To understand the change in the coefficient of friction, an adhesion model based on the boundary element method is employed and shown to capture the dependence of the coefficient of friction on relative humidity at humidities above 20%. The reduction in friction with increasing relative humidity originates from the decrease in capillary adhesion with increasing relative humidity due to the drop in Laplace pressure. The strong decrease in friction with decreasing relative humidity in the low relative humidity regime is attributed to the lack of capillary adhesion and the reduced effect of interfacial bonding by the hydrogen-bond network of water between the interfaces, as evidenced by the velocity-dependent friction experiments. Our results indicate that interfacial hydrogen bonding during sliding contributes to friction.

Acknowledgments We are grateful for financial support from the MaxWater Initiative of the Max Planck Society

Supplementary Information

Hysteresis in the relation between friction and humidity, as shown in Fig. S.1, appears when the friction system is not fully dried before changing the humidity inside the chamber. Such hysteresis is believed to be due to the residual water trapped at the interface. This remaining water could enhance the capillary adhesion at the interface, thereby increasing the friction based on Amonton's law as the capillary adhesion contributes an additional normal force and the friction force is proportional to the normal force. Once the residual water is removed by longtime nitrogen drying, the hysteresis could be eliminated as shown by point 10 in Fig. S.1. What's more, the speed at which the CoF reaches a steady state in Fig. S.2 also indicates the influence of residual water on friction: the CoF reaches a steady state faster after a small change in relative humidity when the sphere is kept in contact with the wafer. In contrast, the CoF could reach a steady state at almost the same speed with surface separation during drying.

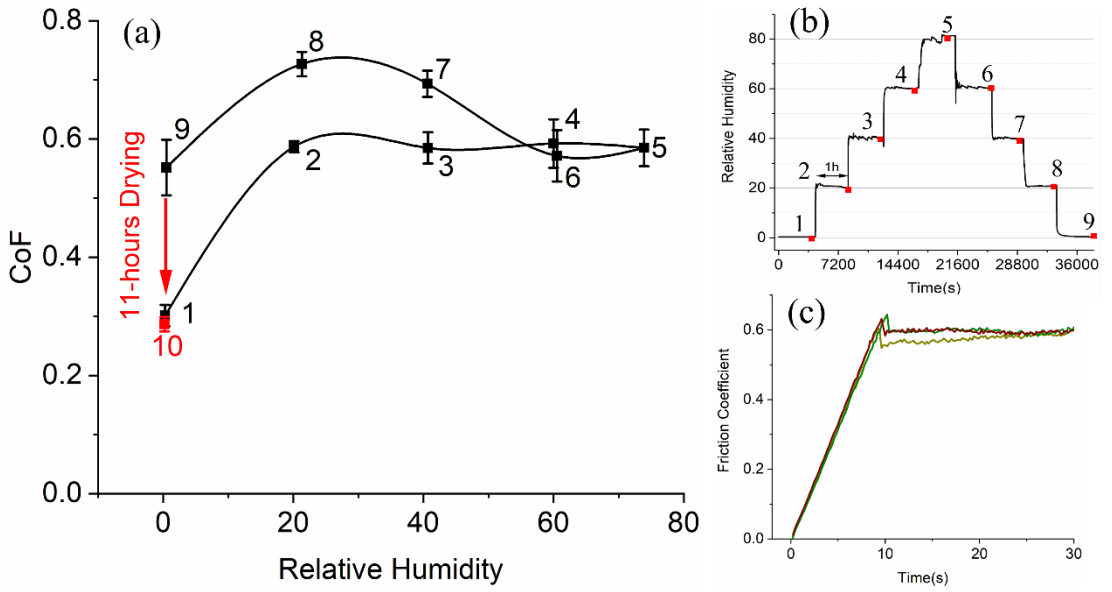

Fig.S1 Friction coefficient hysteresis loop as a function of relative humidity (a). In total ten sets of friction experiments were performed. The corresponding humidity-time curve and the times at which friction experiments were conducted are marked with red dots and numbers in (b). (c) is one example of how the friction coefficient is defined in the steady state at 20% humidity.

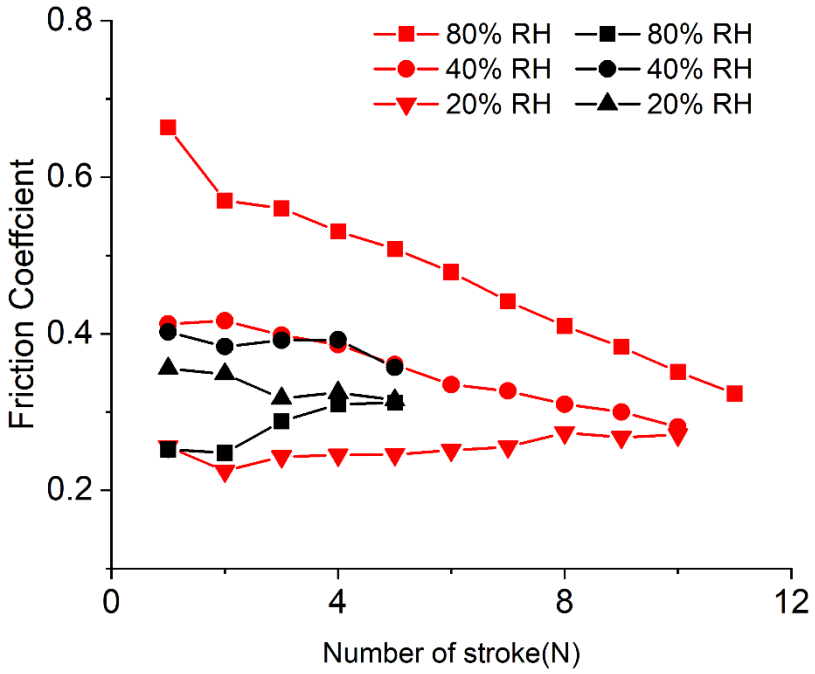

Fig.S2 Friction coefficient as a function of the number of strokes measured after drying the system for one hour. The black solid and red solid lines indicate the situation with (black) and without (red) contact separation after sliding in a specific humidity environment.

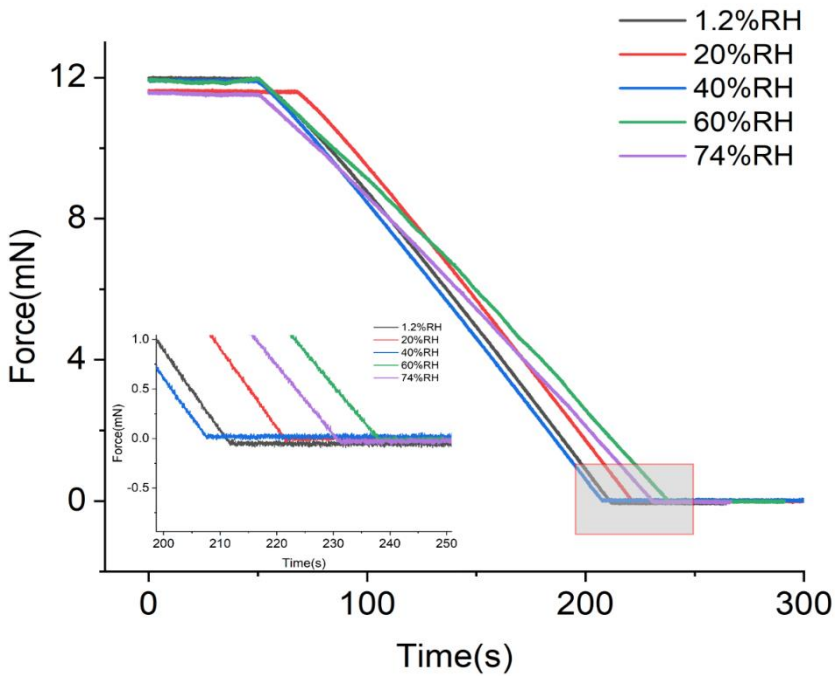

Fig.S3 Forces a function of time measured during the retraction of a wafer from a silicon sphere, the inset shows the force near the contact separation point.

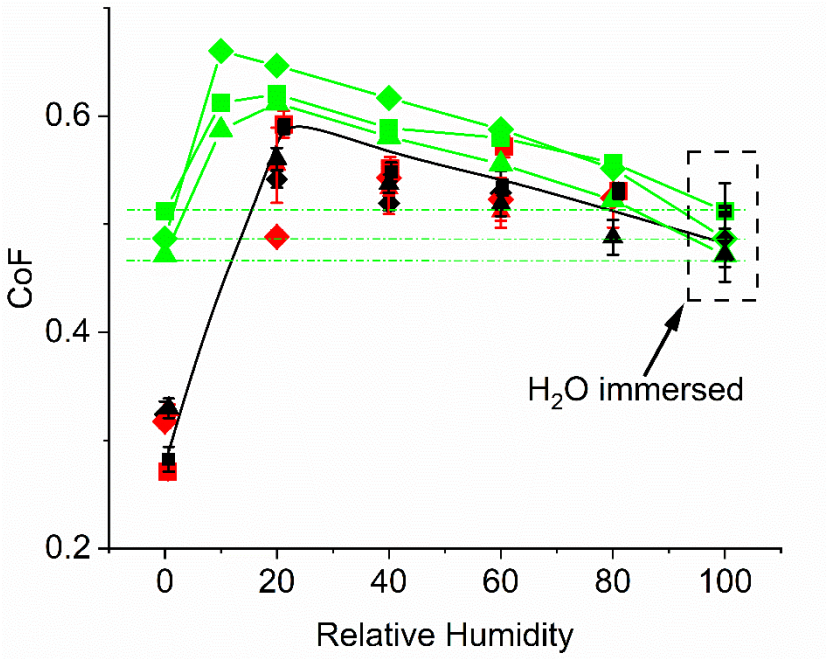

Fig.S4 Calculated and measured coefficient of friction as a function of relative humidity. The red and black symbols indicate friction experiments conducted at increasing (black) and decreasing (red) relative humidity varying from 0.6% to 80%. Squares, triangles and diamonds each correspond to an experiment conducted with a different sphere. The corresponding simulation results are represented by matching green symbols.

Young's modulus (GPa)	Poisson's ratio	Hardness (GPa)
130	0.2	10

Table S1. Mechanical properties of the Si ball and the Si wafer.

Relative humidity	Given elastic repulsive force, $F_{elastic}$ (mN)	Thickness (nm)	Nucleation distance, D (nm)	Simulated capillary adhesion, $F_{simulated}^{adhesion}$ (mN)
10%	53.53	0.35	1.17	9.55
20%	56.24	0.55	1.47	10.25
40%	51.93	0.89	2.07	7.24
60%	53.81	1.23	3.12	6.50
80%	52.15	1.52	5.39	4.28

Table S2. Absorbed water film thickness and nucleation distance in various relative humidities.

Reference

[1] Barnette AL, Ohlhausen JA, Dugger MT, Kim SH. Humidity effects on in situ vapor phase lubrication with n-pentanol. Tribol Lett 2014;55:177–86. https://doi.org/10.1007/s11249-014-

0345-9.

[2] Scherge M, Li X, Schaefer JA. The effect of water on friction of MEMS. Tribol Lett 1999;6:215–20. https://doi.org/10.1023/a:1019119925494.

[3] Chen L, Xiao C, Yu B, Kim SH, Qian L. What Governs Friction of Silicon Oxide in Humid Environment: Contact Area between Solids, Water Meniscus around the Contact, or Water Layer Structure? Langmuir 2017;33(38). https://doi.org/10.1021/acs.langmuir.7b02491.

[4] Hsia F-C, Franklin S, Audebert P, Brouwer AM, Bonn D, Weber B. Rougher is more slippery: How adhesive friction decreases with increasing surface roughness due to the suppression of capillary adhesion. Phys Rev Res 2021;3. https://doi.org/10.1103/physrevresearch.3.043204.

[5] Hsia F, Hsu C, Peng L, Elam FM, Xiao C, Franklin S, et al. Contribution of capillary adhesion to friction at macroscopic solid-solid interfaces. Phys Rev Appl 2022:Accepted.

[6] Asay DB, Kim SH. Effects of adsorbed water layer structure on adhesion force of silicon oxide nanoasperity contact in humid ambient. J Chem Phys 2006;124. https://doi.org/10.1063/1.2192510.

[7] He M, Szuchmacher Blum A, Aston DE, Buenviaje C, Overney RM, Luginbühl R. Critical phenomena of water bridges in nanoasperity contacts. J Chem Phys 2001;114:1355–60. https://doi.org/10.1063/1.1331298.

[8] Seppä J, Reischl B, Sairanen H, Korpelainen V, Husu H, Heinonen M, et al. Atomic force microscope adhesion measurements and atomistic molecular dynamics simulations at different humidities. Meas Sci Technol 2017;28. https://doi.org/10.1088/1361-6501/28/3/034004.

[9] Hasz K, Ye Z, Martini A, Carpick RW. Experiments and simulations of the humidity dependence of friction between nanoasperities and graphite: The role of interfacial contact quality. Phys Rev Mater 2018;2:1–9. https://doi.org/10.1103/PhysRevMaterials.2.126001.

[10] Asay DB, De Boer MP, Kim SH. Equilibrium vapor adsorption and capillary force: Exact laplace-young equation solution and circular approximation approaches. J Adhes Sci Technol 2010;24:2363–82. https://doi.org/10.1163/016942410X508271.

[11] Farshchi-Tabrizia M, Kappl M, Butt HJ. Influence of humidity on adhesion: An atomic force microscope study. J Adhes Sci Technol 2008;22:181–203. https://doi.org/10.1163/156856108X306948.

[12] Asay DB, Kim SH. Effects of adsorbed water layer structure on adhesion force of silicon oxide nanoasperity contact in humid ambient. J Chem Phys 2006;124. https://doi.org/10.1063/1.2192510.

[13] Chen L, Qian L. Role of interfacial water in adhesion, friction, and wear—A critical review. Friction 2021;9:1–28. https://doi.org/10.1007/s40544-020-0425-4.

[14] Pakpour M, Habibi M, Møller P, Bonn D. How to construct the perfect sandcastle. Sci Rep 2012;2:2–4. https://doi.org/10.1038/srep00549.

[15] Fall A, Weber B, Pakpour M, Lenoir N, Shahidzadeh N, Fiscina J, et al. Sliding friction on wet and dry sand. Phys Rev Lett 2014;112. https://doi.org/10.1103/PhysRevLett.112.175502.

[16] Møller PCF, Bonn D. The shear modulus of wet granular matter. Epl 2007;80. https://doi.org/10.1209/0295-5075/80/38002.

[17] Riedo E, Lévy F, Brune H. Kinetics of capillary condensation in nanoscopic sliding friction. Phys Rev Lett 2002;88:1855051–4. https://doi.org/10.1103/physrevlett.88.185505.

[18] Bazrafshan M, de Rooij MB, Schipper DJ. Adhesive force model at a rough interface in the presence of thin water films: The role of relative humidity. Int J Mech Sci 2018;140:471–85.

https://doi.org/10.1016/j.ijmecsci.2018.03.024.

[19] Noel O, Mazeran PE, Nasrallah H. Sliding velocity dependence of adhesion in a nanometer-sized contact. Phys Rev Lett 2012;108:1–4. https://doi.org/10.1103/PhysRevLett.108.015503.

[20] DelRio FW, Dunn ML, Phinney LM, Bourdon CJ, De Boer MP. Rough surface adhesion in the presence of capillary condensation. Appl Phys Lett 2007;90. https://doi.org/10.1063/1.2723658.

[21] Soylemez E, De Boer MP. Modeling capillary bridge dynamics and crack healing between surfaces of nanoscale roughness. J Micromechanics Microengineering 2017;27. https://doi.org/10.1088/1361-6439/aa98c3.

[22] Thimons LA, Gujrati A, Sanner A, Pastewka L, Jacobs TDB. Hard-material Adhesion: Which Scales of Roughness Matter? Exp Mech 2021;61:1109–20. https://doi.org/10.1007/s11340-021-00733-6.

[23] Persson BNJ, Albohr O, Tartaglino U, Volokitin AI, Tosatti E. On the nature of surface roughness with application to contact mechanics, sealing, rubber friction and adhesion. J Phys Condens Matter 2005;17. https://doi.org/10.1088/0953-8984/17/1/R01.

[24] Tiwari A, Wang J, Persson BNJ. Adhesion paradox: Why adhesion is usually not observed for macroscopic solids. Phys Rev E 2020;102:42803. https://doi.org/10.1103/PhysRevE.102.042803.

[25] Leriche C, Franklin S, Weber B. Measuring multi-asperity wear with nanoscale precision. Wear 2022:204284. https://doi.org/10.1016/j.wear.2022.204284.

[26] Hsia FC, Elam FM, Bonn D, Weber B, Franklin SE. Wear particle dynamics drive the difference between repeated and non-repeated reciprocated sliding. Tribol Int 2020;142:105983. https://doi.org/10.1016/j.triboint.2019.105983.

[27] Kim S, Kim D, Kim J, An S, Jhe W. Direct Evidence for Curvature-Dependent Surface Tension in Capillary Condensation: Kelvin Equation at Molecular Scale. Phys Rev X 2018;8:41046. https://doi.org/10.1103/PhysRevX.8.041046.

[28] Xiao C, Chen C, Yao Y, Liu H, Chen L, Qian L, et al. Nanoasperity Adhesion of the Silicon Surface in Humid Air: The Roles of Surface Chemistry and Oxidized Layer Structures. Langmuir 2020;36:5483–91. https://doi.org/10.1021/acs.langmuir.0c00205.

[29] Berman A, Drummond C, Israelachvili J. Amontons' law at the molecular level. Tribol Lett 1998;4:95–101. https://doi.org/10.1023/A:1019103205079.

[30] Israelachvili J, Giasson S, Kuhl T, Drummond C, Berman A, Luengo G, et al. Some fundamental differences in the adhesion and friction of rough versus smooth surfaces. vol. 38. Elsevier Masson SAS; 2000. https://doi.org/10.1016/s0167-8922(00)80107-8.

[31] He X, Liu Z, Ripley LB, Swensen VL, Griffin-Wiesner IJ, Gulner BR, et al. Empirical relationship between interfacial shear stress and contact pressure in micro- and macro-scale friction. Tribol Int 2021;155:106780. https://doi.org/10.1016/j.triboint.2020.106780.

[32] Hasz K, Ye Z, Martini A, Carpick RW. Experiments and simulations of the humidity dependence of friction between nanoasperities and graphite: The role of interfacial contact quality. Phys Rev Mater 2018;2:1–9. https://doi.org/10.1103/PhysRevMaterials.2.126001.

[33] Wang X, Kim SH, Chen C, Chen L, He H, Qian L. Humidity dependence of tribochemical wear of monocrystalline silicon. ACS Appl Mater Interfaces 2015;7:14785–92. https://doi.org/10.1021/acsami.5b03043.

[34] Chen C, Xiao C, Wang X, Zhang P, Chen L, Qi Y, et al. Role of water in the tribochemical removal of bare silicon. Appl Surf Sci 2016;390:696–702. https://doi.org/10.1016/j.apsusc.2016.08.175.

[35] Tong Q -Y., Lee T -H., Gösele U, Reiche M, Ramm J, Beck E. The Role of Surface Chemistry in Bonding of Standard Silicon Wafers. J Electrochem Soc 1997;144:384–9. https://doi.org/10.1149/1.1837415.

[36] Plach T, Hingerl K, Tollabimazraehno S, Hesser G, Dragoi V, Wimplinger M. Mechanisms for room temperature direct wafer bonding. J Appl Phys 2013;113. https://doi.org/10.1063/1.4794319.

[37] Yu J, Kim SH, Yu B, Qian L, Zhou Z. Role of tribochemistry in nanowear of single-crystalline silicon. ACS Appl Mater Interfaces 2012;4:1585–93. https://doi.org/10.1021/am201763z.

[38] Schott H. Direct Comparison of the Strength of Hydrogen Bonds Formed by H2O and D2O. J Macromol Sci Part B 1988;27:119–23. https://doi.org/10.1080/00222348808212315.

[39] Scheiner S, Čuma M. Relative stability of hydrogen and deuterium bonds. J Am Chem Soc 1996;118:1511–21. https://doi.org/10.1021/ja9530376.

[40] Tarmian A, Burgert I, Thybring EE. Hydroxyl accessibility in wood by deuterium exchange and ATR-FTIR spectroscopy: methodological uncertainties. Wood Sci Technol 2017;51:845–53. https://doi.org/10.1007/s00226-017-0922-9.

[41] Némethy G, Scheeaga HA. Structure of water and hydrophobic bonding in proteins. I. A model for the thermodynamic properties of liquid water. J Chem Phys 1962;36:3382–400. https://doi.org/10.1063/1.1732472.

[42] Batteas JD, Quan X, Weldon MK. Adhesion and wear of colloidal silica probed by force microscopy. Tribol Lett 1999;7:121–8. https://doi.org/10.1023/a:1019125521376.

[43] Cleaver J. Bonding and Interparticle Interactions of Silica Nanoparticles. vol. 37. 2004. https://doi.org/10.1016/j.triboint.2004.02.001.

[44] Bar-sinai Y, Spatschek R, Brener E a, Bouchbinder E. On the velocity-strengthening behavior of dry friction 2014;2014:1738–48. https://doi.org/10.1002/2013JB010586.Abstract.

[45] Chen J, Ratera I, Park JY, Salmeron M. Velocity dependence of friction and hydrogen bonding effects. Phys Rev Lett 2006;96:2–5. https://doi.org/10.1103/PhysRevLett.96.236102.

[46] Nicodemus RA, Corcelli SA, Skinner JL, Tokmakoff A. Collective hydrogen bond reorganization in water studied with temperature-dependent ultrafast infrared spectroscopy. J Phys Chem B 2011;115:5604–16. https://doi.org/10.1021/jp111434u.